materials

MDPI

Article

Polyoxomolybdate Layered Crystals Constructed from a Heterocyclic Surfactant: Syntheses, Pseudopolymorphism and Introduction of Metal Cations

Jun Kobayashi [1], Keisuke Shimura [1], Keisuke Mikurube [1], Saki Otobe [1], Takashi Matsumoto [2], Eri Ishikawa [3], Haruo Naruke [4] and Takeru Ito [1,*]

[1] Department of Chemistry, School of Science, Tokai University, Kanagawa 259-1292, Japan; j.koba92@gmail.com (J.K.); dohc.supertracker@gmail.com (K.S.); k_m0423_tokai@yahoo.co.jp (K.M.); sob0406qwer@gmail.com (S.O.)
[2] Application Laboratories, Rigaku Corporation, Tokyo 196-8666, Japan; t-matumo@rigaku.co.jp
[3] Department of Applied Chemistry, College of Engineering, Chubu University, Aichi 487-8501, Japan; eishikawa@isc.chubu.ac.jp
[4] Chemical Resources Laboratory, Tokyo Institute of Technology, Kanagawa 226-8503, Japan; hnaruke@gmail.com
* Correspondence: takeito@keyaki.cc.u-tokai.ac.jp

Abstract: Crystals with layered structures are crucial for the construction of functional materials exhibiting intercalation, ionic conductivity, or emission properties. Polyoxometalate crystals hybridized with surfactant cations have distinct layered packings due to the surfactants which can form lamellar structures. Introducing metal cations into such polyoxometalate-surfactant hybrid crystals is significant for the addition of specific functions. Here, polyoxomolybdate–surfactant hybrid crystals were synthesized as single crystals, and unambiguously characterized by X-ray structure analyses. Octamolybdate ($[Mo_8O_{26}]^{4-}$, Mo_8) and heterocyclic surfactant of 1-dodecylpyridinium ($C_{12}py$) were employed. The hybrid crystals were composed of α-type and β-type Mo_8 isomers. Two crystalline phases containing α-type Mo_8 were obtained as pseudopolymorphs depending on the crystallization conditions. Crystallization with the presence of rubidium and cesium cations caused the formation of metal cation-introduced hybrid crystals comprising β-Mo_8 ($C_{12}py$-Rb-Mo_8 and $C_{12}py$-Cs-Mo_8). The yield of the $C_{12}py$-Rb-Mo_8 hybrid crystal was almost constant within crystallization temperatures of 279–303 K, while that of $C_{12}py$-Cs-Mo_8 decreased over 288 K. This means that the $C_{12}py$-Mo_8 hybrid crystal can capture Rb^+ and Cs^+ from the solution phase into the solids as the $C_{12}py$-Rb-Mo_8 and $C_{12}py$-Cs-Mo_8 hybrid crystals. The $C_{12}py$-Mo_8 hybrid crystals could be applied to ion-capturing materials for heavy metal cation removal.

Keywords: polyoxometalate; inorganic-organic hybrid; layered crystal; surfactant; metal cation

check for updates

Citation: Kobayashi, J.; Shimura, K.; Mikurube, K.; Otobe, S.; Matsumoto, T.; Ishikawa, E.; Naruke, H.; Ito, T. Polyoxomolybdate Layered Crystals Constructed from a Heterocyclic Surfactant: Syntheses, Pseudopolymorphism and Introduction of Metal Cations. *Materials* **2022**, *15*, 2429. https://doi.org/10.3390/ma15072429

Academic Editor: Morena Nocchetti

Received: 28 February 2022
Accepted: 23 March 2022
Published: 25 March 2022

1. Introduction

Layered materials comprise two-dimensionally piled chemical components showing distinct structural anisotropy [1]. Such two-dimensional anisotropy induces characteristic properties such as conductivity [2,3], intercalation [4], magnetism [5], or emission capability [6]. Crystalline layered materials possess merits regarding their thermal stability and structural ordering in the long range, which can improve their properties [7–10]. In addition, introduction of metal cations into the crystalline layered materials can provide another function such as uptake of heavy or toxic metal cations [11–13].

To construct functional layered materials, inorganic polyoxometalate (POM) anions [14–18] and surfactant cations [19,20] represent useful components. The molecular-designable POMs and lamellar-forming surfactants can build up precisely controlled layered materials in their structures and functions [21–27]. Selective introduction of metal

cations into the POM–surfactant hybrids can enable the emergence of a desired function such as ionic conductivity or metal cation-capture.

Among several POM–surfactant hybrid systems, POM–surfactant hybrid crystals can tune their crystalline ordered structure and function by selecting a combination of POM anion and surfactant cation [28–38]. Several metal cations (Na^+, K^+, Ag^+, etc.) have been incorporated into polyoxomolybdate hybrid crystals [39–41], which were accompanied with the isomerization of octamolybdate ($[Mo_8O_{26}]^{4-}$, Mo_8) (Scheme 1a). The isomerization often occurs in an acetonitrile solvent [42]. These isomers in the solid state can be identified by infrared (IR) spectra [43,44]. Using heterocyclic pyridinium surfactant is effective for synthesis of Mo_8-surfactant hybrid crystals incorporating metal cations. However, the examples have been limited to crystals consisting of 1-hexadecylpyridinium ($[C_5H_5N(C_{16}H_{33})]^+$, C_{16}py) [39–41], which were obtained in low yields (< 10%) and sometimes in a mixed phase [41].

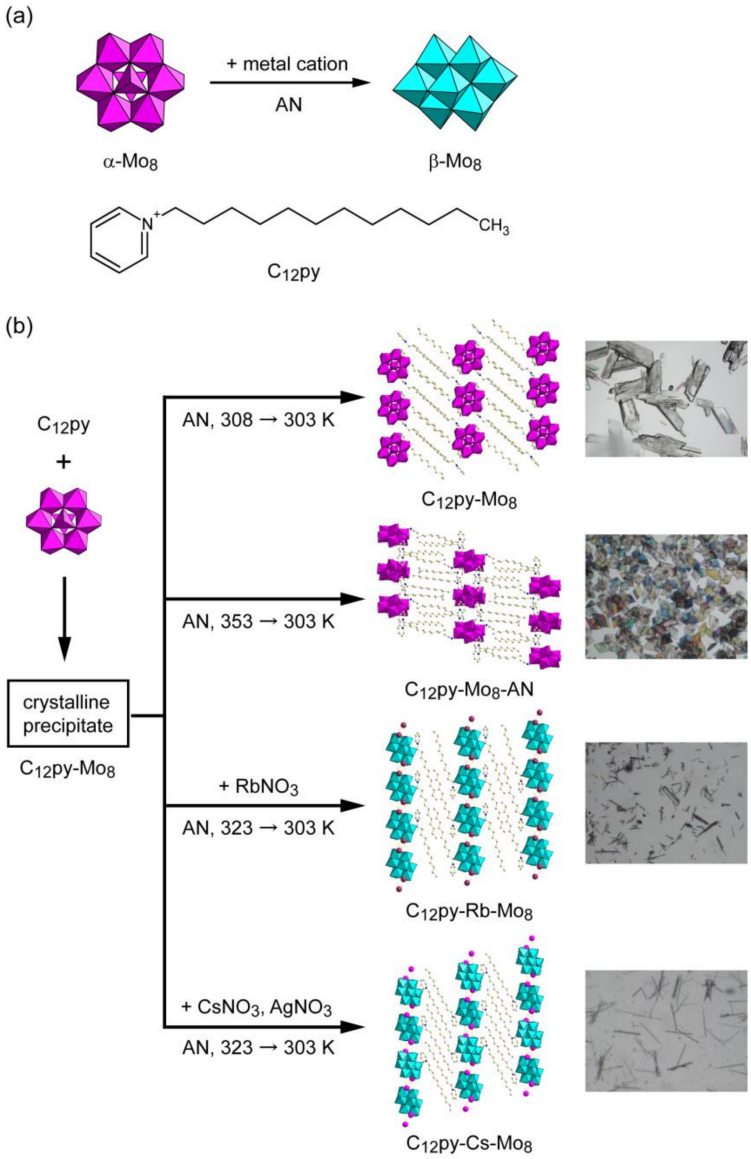

Scheme 1. (**a**) Molecular structure of utilized components. Upper: α- and β-octamolybdate (α- and β-Mo_8) anions isomerizing in acetonitrile (AN) under the presence of metal cation. Bottom: 1-dodecylpyidinium (C_{12}py) cation; (**b**) Schematic procedures of the syntheses of C_{12}py-Mo_8 and related hybrid crystals. Some colorless crystals of C_{12}py-Mo_8-AN were colored in the photograph due to attached polarizing filters.

Here, several Mo_8-surfactant hybrid crystals were successfully obtained by using 1-dodecylpyridinium surfactant ($[C_5H_5N(C_{12}H_{25})]^+$, C_{12}py, Scheme 1a). The shorter alkyl chain of C_{12}py is considered to enhance the solubility and crystallization of C_{12}py-Mo_8 hybrid crystals, and indeed enable the synthesis of several C_{12}py-Mo_8 hybrid crystals in a pure phase and a higher yield (>~30%). In this report, syntheses and pseudopolymorphism of the C_{12}py-Mo_8 hybrid crystals were investigated, and the introduction of metal cations into the C_{12}py-Mo_8 hybrid crystals was achieved with Rb^+ and Cs^+. The temperature dependence of the yield was evaluated for metal cation-introduced C_{12}py-Mo_8 hybrid crystals to assess the possibility of capturing heavy or radioactive metal cations.

2. Materials and Methods

2.1. Genaral Procedures and Instrumental Methods

All chemical reagents were purchased from FUJIFILM Wako Pure Chemical Corporation (Osaka, Japan) and Tokyo Chemical Industry Co., Ltd. (TCI, Tokyo, Japan) and utilized without further purification.

Infrared (IR) spectra were measured on a Jasco FT/IR-4200ST spectrometer (KBr pellet method). Powder X-ray diffraction (XRD) patterns were recorded with a Rigaku MiniFlex300 diffractometer (Cu Kα radiation, λ = 1.54056 Å) at ambient temperature. CHN (carbon, hydrogen and nitrogen) elemental analyses were carried out with a PerkinElmer 2400II elemental analyzer. X-ray fluorescence (XRF) analyses were performed with a Hitachi EA1000AIII XRF analyzer.

2.2. Syntheses of C_{12}py-Mo_8 and Related Hybrid Crystals

2.2.1. C_{12}py-Mo_8

$Na_2MoO_4{\cdot}2H_2O$ (1.5 g, 6.2 mmol) or $(NH_4)_6Mo_7O_{24}{\cdot}4H_2O$ (1.0 g, 0.81 mmol) was dissolved in H_2O (10 mL), and 6M HCl was added to adjust the pH to 3.8. To this solution was added a water/ethanol (10 mL, 1:1 (*v/v*)) solution of C_{12}pyCl·H_2O (0.81 g, 2.7 mmol) and stirred for 10 min. The resulting suspension was filtered and dried in dark conditions to obtain colorless crystalline precipitate of C_{12}py-Mo_8 (0.90–1.2 g, yield 55–70%) (Scheme 1b). An acetonitrile (AN) solution (15 mL) containing the C_{12}py-Mo_8 precipitate (0.03 g) was heated at 308 K for one day, and sequentially the resulting colorless supernatant was stored at 303 K to obtain colorless plate crystals of C_{12}py-Mo_8 (yield ~30%) (Scheme 1b). CHN elemental analysis: Calcd for $C_{72}H_{132}N_4Mo_8O_{28}$: C: 38.11, H: 5.86, N: 2.47%. Found: C: 38.68, H: 5.74, N: 2.52%. IR (KBr disk): 943 (s), 913 (s), 845 (m), 804 (m), 777 (m), 714 (s), 686 (m), 664 (m), 646 (m), 556 (w), 520 (m), 487 (w), 472 (w), 454 (w), 443 (w), 412 (w) cm^{-1}. The single crystals of C_{12}py-Mo_8 were also obtained by gradual reoxidation of reduced molybdenum POM species (C_{12}py-red-Mo, see Supplementary Materials).

2.2.2. C_{12}py-Mo_8-AN

An acetonitrile (AN) solution (15 mL) containing the crystalline precipitate of C_{12}py-Mo_8 (0.03 g) was heated at 353 K for 3 h. The resultant colorless supernatant was kept at 303 K to obtain colorless plate crystals of C_{12}py-Mo_8-AN (yield ~30%) (Scheme 1b). Better single crystals were crystallized from the C_{12}py-Mo_8 precipitate synthesized with $(NH_4)_6Mo_7O_{24}{\cdot}4H_2O$. Solvent molecules of crystallization were easily removed under ambient atmosphere. CHN elemental analysis: Calcd for $C_{68}H_{120}N_4Mo_8O_{26}$: C: 37.51, H: 5.56, N: 2.57%. Found: C: 37.21, H: 5.37, N: 2.70%. IR (KBr disk): 953 (w), 910 (s), 847 (m), 805 (s), 720 (w), 662 (s), 556 (w), 505 (w), 477 (w), 457 (w), 421 (w) cm^{-1}.

2.2.3. C_{12}py-Rb-Mo_8

An acetonitrile (AN) solution (15 mL) containing the crystalline precipitate of C_{12}py-Mo_8 (0.03 g) and solid $RbNO_3$ (0.02 g) was heated at 323 K for 1 day. The resulting colorless supernatant was kept at 303 K to obtain colorless needle crystals of C_{12}py-Rb-Mo_8 (yield ~25%) (Scheme 1b). The yield of the C_{12}py-Rb-Mo_8 crystals was estimated based on the mass of added $RbNO_3$ by changing the keeping temperature (279, 288, 293, 303 K). XRF

analysis confirmed the atomic ratio of Rb:Mo to be 2:8. CHN elemental analysis: Calcd for $C_{34}H_{60}N_2Rb_2Mo_8O_{26}$: C: 22.06, H: 3.27, N: 1.51%. Found: C: 21.86, H: 3.04, N: 1.51%. IR (KBr disk): 951 (s), 942 (s), 903 (s), 844 (s), 725 (s), 680 (m), 653 (m), 578 (w), 555 (w), 524 (w), 479 (w), 448 (w), 409 (w) cm^{-1}.

2.2.4. C_{12}py-Cs-Mo_8

Colorless needles of C_{12}py-Rb-Mo_8 were obtained by a similar procedure for C_{12}py-Rb-Mo_8 (yield ~10%) (Scheme 1b). Solid $CsNO_3$ (0.02 g) and $AgNO_3$ (0.02 g) were employed instead of $RbNO_3$. The yield of the C_{12}py-Cs-Mo_8 crystals was estimated based on the mass of added $CsNO_3$ by changing the keeping temperature (279, 288, 293, 303 K). XRF analysis confirmed the atomic ratio of Cs:Mo to be 2:8. CHN elemental analysis: Calcd for $C_{34}H_{60}N_2Cs_2Mo_8O_{26}$: C: 20.98, H: 3.11, N: 1.44%. Found: C: 20.88, H: 3.11, N: 1.58%. IR (KBr disk): 953 (m), 942 (s), 906 (s), 848 (m), 773 (w), 732 (m), 659 (m), 553 (w), 525 (w), 475 (w), 434 (w) cm^{-1}.

2.3. X-ray Crystallography

Single crystal X-ray diffraction data for C_{12}py-Mo_8 were measured on a Rigaku XtaLAB P200 diffractometer by using graphite monochromated Mo Kα radiation. The diffraction data were collected with CrystalClear [45] and processed with CrysAlisPro [46]. Diffraction data for C_{12}py-Mo_8-AN and C_{12}py-Rb-Mo_8 were collected and processed on a Rigaku R-AXIS RAPID diffractometer by using graphite monochromated Mo Kα radiation with PROCESS-AUTO [47]. Diffraction data for C_{12}py-Cs-Mo_8 were measured on a Rigaku Saturn70 diffractometer using multi-layer mirror monochromated Mo Kα radiation. The diffraction data were collected with CrystalClear and processed with CrysAlisPro.

Crystal structures except for C_{12}py-Mo_8-AN were solved by SHELXT (Version 2014/5 or 2018/2) [48], and the structure of C_{12}py-Mo_8-AN by SIR92 [49]. The refinement procedure was performed by the full-matrix least-squares using SHELXL (Version 2018/3) [50] through CrystalStructure software package [51]. Non-hydrogen atoms were refined anisotropically, and the hydrogen atoms on carbon atoms were located in calculated positions.

3. Results

3.1. Syntheses of a Series of C_{12}py-Mo_8 Hybrid Crystals

Crystalline precipitate of C_{12}py-Mo_8 was obtained in 55–70% yield (based on Mo) by the reaction using acidified aqueous solution (pH = 3.8) of Mo_8 species and C_{12}py cation. The IR spectrum of C_{12}py-Mo_8 precipitate (Figure 1a) shows characteristic peaks owing to α-Mo_8 [42–44] in the range of 400–1000 cm^{-1} together with the peaks of C_{12}py (pyridine ring in 1400–1500 cm^{-1} and methylene groups in 2800–3000 cm^{-1}), demonstrating the successful hybridization of α-Mo_8 anion and C_{12}py cation. The peaks in the 910–960 cm^{-1} range could be assigned to terminal Mo=O vibrations relevant to MoO_6 unit [52–54]. The peaks in the 400–880 cm^{-1} range could be due to Mo-O-Mo vibrations. The peaks around 805 cm^{-1} may be attributed to Mo-O vibrations of MoO_4 unit [53]. The obtained C_{12}py-Mo_8 precipitate was highly crystalline as judged from the powder XRD pattern (Figure 2a) and did not depend on the difference in the molybdenum sources. The C_{12}py-Mo_8 precipitate was successfully recrystallized as single crystals from the acetonitrile solution (Scheme 1b), which was supported by similar IR spectra (Figure 1a,b) and powder XRD patterns (Figure 2a,b) of C_{12}py-Mo_8 before and after the recrystallization.

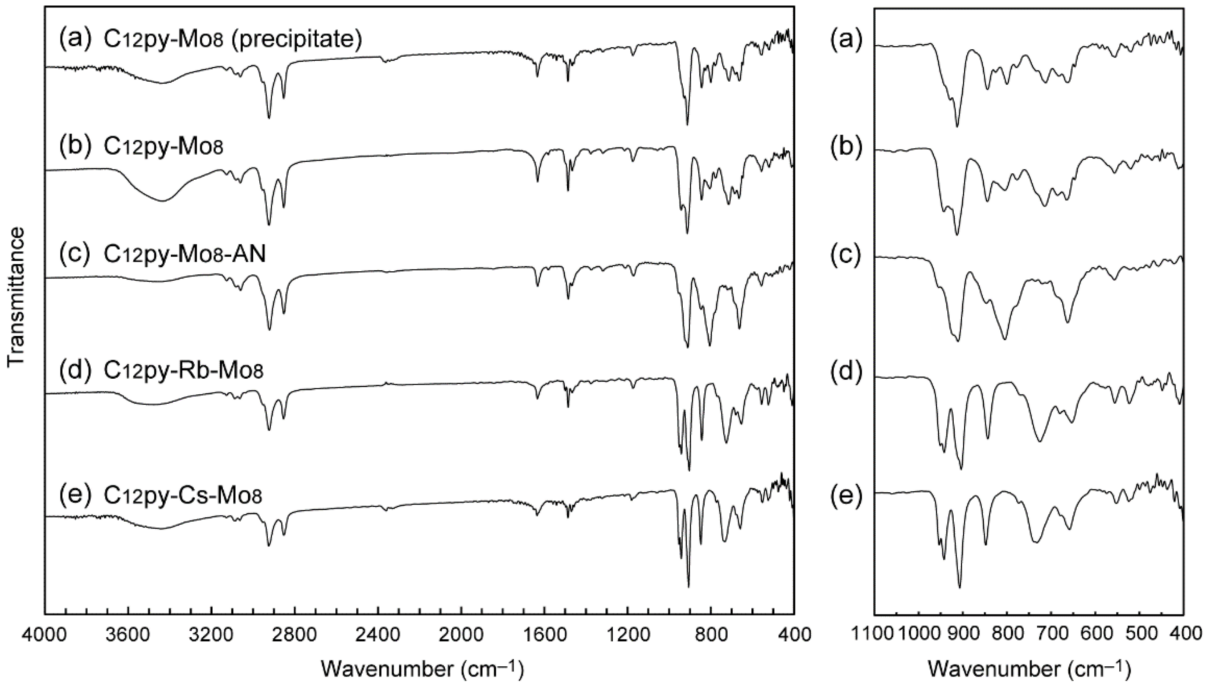

Figure 1. IR spectra of C_{12}py-Mo_8 and related hybrid crystals: (**a**) C_{12}py-Mo_8 precipitate; (**b**) C_{12}py-Mo_8 after recrystallization; (**c**) C_{12}py-Mo_8-AN; (**d**) C_{12}py-Rb-Mo_8; (**e**) C_{12}py-Cs-Mo_8.

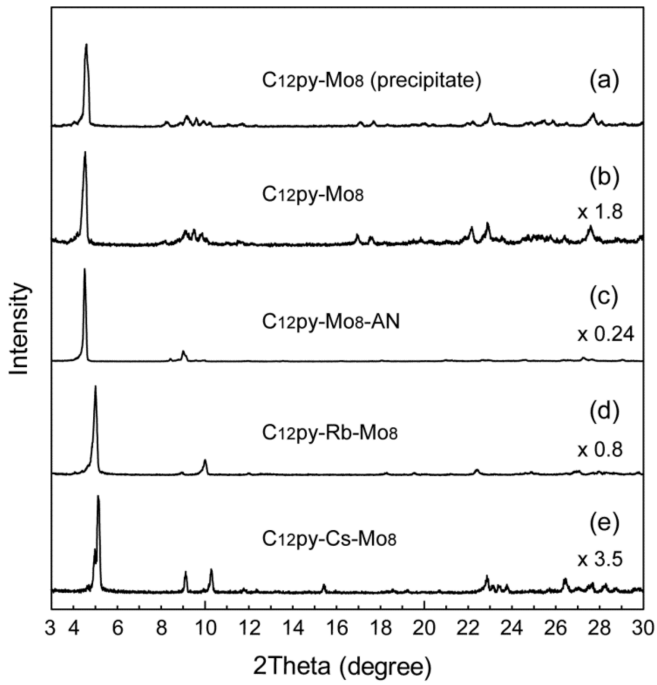

Figure 2. Powder XRD patterns of C_{12}py-Mo_8 and related hybrid crystals: (**a**) C_{12}py-Mo_8 precipitate; (**b**) C_{12}py-Mo_8 after recrystallization; (**c**) C_{12}py-Mo_8-AN; (**d**) C_{12}py-Rb-Mo_8; (**e**) C_{12}py-Cs-Mo_8.

Another hybrid crystal of C_{12}py-Mo_8-AN was obtained from the starting C_{12}py-Mo_8 precipitate under different crystallization conditions (different heating temperature of 353 K, Scheme 1b). The IR spectrum of C_{12}py-Mo_8-AN (Figure 1c) indicates the presence of the α-Mo_8 anion hybridized with the C_{12}py cation. However, both IR spectrum and powder XRD pattern (Figure 2c) for C_{12}py-Mo_8-AN were slightly different from those of C_{12}py-Mo_8 (Figure 1a,b and Figure 2a,b), suggesting the formation of a different crystalline

phase from C_{12}py-Mo_8. The emergence of a different phase was revealed by single crystal structure analyses (see below).

Hybrid crystals of C_{12}py-Rb-Mo_8 and C_{12}py-Rb-Mo_8 were obtained under the presence of Rb^+ and Cs^+ cations (Scheme 1b). Their IR spectra exhibit characteristic peaks of β-Mo_8 (400–1000 cm^{-1}) [42–44] as well as the peaks of C_{12}py (1400–1500 and 2800–3000 cm^{-1}) as shown in Figure 1d,e, indicating that the β-Mo_8 anion existed in the obtained hybrid crystals. This implies that the isomerization of α-Mo_8 to β-Mo_8 occurred during the crystallization process [41], which was supported by single crystal structure analyses (see below). The peaks in the 910–960 cm^{-1} and 400–880 cm^{-1} range could be attributed to terminal Mo=O and Mo-O-Mo vibrations of MoO_6 units in β-Mo_8, respectively [52–54]. The distinct peaks around 655 and 730 cm^{-1} may suggest the presence of a two-dimensional connection between β-Mo_8 anions and metal cations [42–44].

For all these hybrid crystals, the measured powder XRD patterns were similar to those calculated from the single crystal structure analyses (Figure S1). This demonstrates that each C_{12}py-Mo_8 hybrid crystal was obtained essentially as a pure phase. C_{12}py-Cs-Mo_8 may contain a minor phase with a different layer distance due to the different alkyl chain conformation in C_{12}py. Slight differences in the reflection peak position and intensity of the measured and calculated patterns will be derived from the different measurement temperatures (powder: ambient temperature, single crystal: 93 or 193 K), and from preferred orientation due to the distinct layered structures.

3.2. Crystal Structures of C_{12}py-Mo_8 Hybrid Crystals

Crystalline precipitate of C_{12}py-Mo_8 was successfully recrystallized with hot acetonitrile as mentioned above. The formula was revealed to be $[C_5H_5(C_{12}H_{25})]_4[\alpha\text{-}Mo_8O_{26}]$ by the single crystal X-ray and CHN elemental analyses (Table 1). Four C_{12}py cations (1+ charge) and one α-Mo_8 anion (4- charge) were associated to compensate the opposite charges. Another type of counter cation or solvent of crystallization was not included. C_{12}py-Mo_8 exhibited a distinct layered structure consisting of α-Mo_8 monolayers and C_{12}py interdigitated bilayers with a periodicity of 19.0 Å (Figure 3a). This C_{12}py-Mo_8 phase was also obtained by gradual reoxidation of C_{12}py-red-Mo (Table S1, Figures S2 and S3).

Crystalline phase of C_{12}py-Mo_8-AN was obtained from the same starting precipitate of C_{12}py-Mo_8 under the different heating temperature (Scheme 1b). The formula of C_{12}py-Mo_8-AN was $[C_5H_5(C_{12}H_{25})]_4[\alpha\text{-}Mo_8O_{26}]\cdot CH_3CN$, which consisted of one α-Mo_8 anion, four C_{12}py cations, and one additional acetonitrile of crystallization (Figure 3b). The compositional difference between C_{12}py-Mo_8-AN and C_{12}py-Mo_8 was only in the presence of crystallization solvent, which means that the hybrid crystal of C_{12}py-Mo_8-AN was a pseudopolymorph of C_{12}py-Mo_8. C_{12}py-Mo_8-AN contained alternate stacking of α-Mo_8 monolayers and C_{12}py bilayers with an interlayer distance of 19.4 Å. The acetonitrile molecules of crystallization were located at the interface between the α-Mo_8 and C_{12}py layers

Each α-Mo_8 anion in C_{12}py-Mo_8 and C_{12}py-Mo_8-AN was isolated by the pyridine rings inserted into the inorganic layers (Figure 3c,d). There was one crystallographically-independent α-Mo_8 anion in C_{12}py-Mo_8, while there were two crystallographically-independent α-Mo_8 anions in C_{12}py-Mo_8-AN, resulting in the different molecular conformation of α-Mo_8 in the C_{12}py-Mo_8 and C_{12}py-Mo_8-AN hybrid crystals (Figure 3c,d). This difference and the presence of acetonitrile in the vicinity of α-Mo_8 may lead to a slightly different IR spectrum of C_{12}py-Mo_8-AN (Figure 1c) from C_{12}py-Mo_8 (Figure 1a,b) [55].

Table 1. Crystallographic data.

Compound	C_{12}py-Mo_8	C_{12}py-Mo_8-AN	C_{12}py-Rb-Mo_8	C_{12}py-Cs-Mo_8
Chemical formula	$C_{68}H_{120}N_4Mo_8O_{26}$	$C_{70}H_{123}N_5Mo_8O_{26}$	$C_{34}H_{60}N_2Rb_2Mo_8O_{26}$	$C_{34}H_{60}N_2Cs_2Mo_8O_{26}$
Formula weight	2177.23	2218.28	1851.30	1946.18
Crystal system	triclinic	triclinic	triclinic	triclinic
Space group	$P\bar{1}$ (No. 2)	$P\bar{1}$ (No. 2)	$P\bar{1}$ (No. 2)	$P\bar{1}$ (No. 2)
a (Å)	10.3430(5)	12.8469(8)	7.8864(4)	7.9663(3)
b (Å)	11.3843(6)	18.0395(10)	10.6302(4)	17.4100(5)
c (Å)	19.7519(11)	20.5427(12)	17.7431(10)	20.3300(6)
α (°)	79.308(5)	108.6372(12)	91.918(3)	75.492(3)
β (°)	76.042(4)	94.6749(15)	98.1055(19)	88.785(3)
γ (°)	70.315(4)	90.4647(14)	111.357(3)	85.313(3)
V (Å^3)	2111.3(2)	4493.2(5)	1365.68(12)	2720.59(16)
Z	1	2	1	2
ρ_{calcd} (g·cm^{-3})	1.712	1.639	2.251	2.376
T (K)	93	193	193	193
Wavelength (Å)	0.71073	0.71075	0.71075	0.71073
μ (mm^{-1})	1.219	1.148	3.619	3.178
No. of reflections measured	32,803	66,871	22,036	21,492
No. of independent reflections	16,306	20,485	6242	12,476
R_{int}	0.0830	0.0485	0.0485	0.0445
No. of parameters	480	1315	418	652
R_1 ($I > 2\sigma(I)$)	0.0554	0.0494	0.0313	0.0543
wR_2 (all data)	0.0906	0.0904	0.0606	0.1395

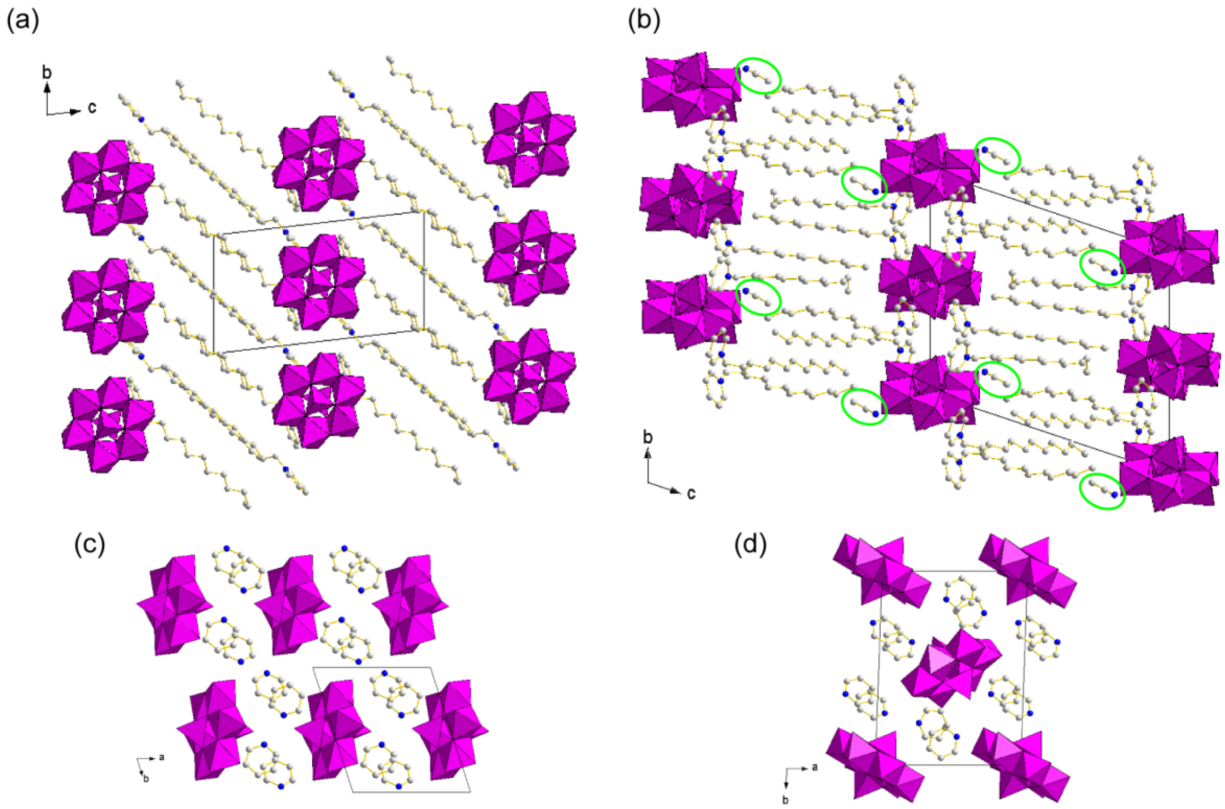

Figure 3. Crystal structures of C_{12}py-Mo_8 and C_{12}py-Mo_8-AN (C: gray, N: blue; α-Mo_8 in purple polyhedrons). H atoms and disordered atoms are omitted for clarity: (**a**) Packing diagram of C_{12}py-Mo_8 along the *a* axis; (**b**) Packing diagram of C_{12}py-Mo_8-AN along the *a* axis. Some solvent molecules are highlighted by green ovals; (**c**) Molecular arrangements of C_{12}py-Mo_8 in the inorganic layers (*ab* plane); (**d**) Molecular arrangements of C_{12}py-Mo_8-AN in the inorganic layers (*ab* plane).

3.3. Crystal Structures of Metal Cation-Introduced Hybrid Crystals Derived from C_{12}py-Mo_8

Crystallization of the C_{12}py-Mo_8 precipitate under the presence of metal cations led to the formation of hybrid crystals in which the corresponding metal cation was introduced (Scheme 1b). Rb^+ and Cs^+ were successfully incorporated into the hybrid crystals as shown in Table 1 and Figure 4. The chemical formulae of C_{12}py-Rb-Mo_8 and C_{12}py-Cs-Mo_8 were $[C_5H_5N(C_{12}H_{25})]_2Rb_2[\beta\text{-}Mo_8O_{26}]$ and $[C_5H_5N(C_{12}H_{25})]_2Cs_2[\beta\text{-}Mo_8O_{26}]$, respectively. Both metal cation-introduced hybrid crystals contained the β-Mo_8 anion as indicated by the IR spectra (Figure 1d,e). Two C_{12}py cations (1+ charge) and two Rb^+ and Cs^+ were associated with one β-Mo_8 anion (4− charge) due to charge compensation. No solvent molecule was included in the crystal structures.

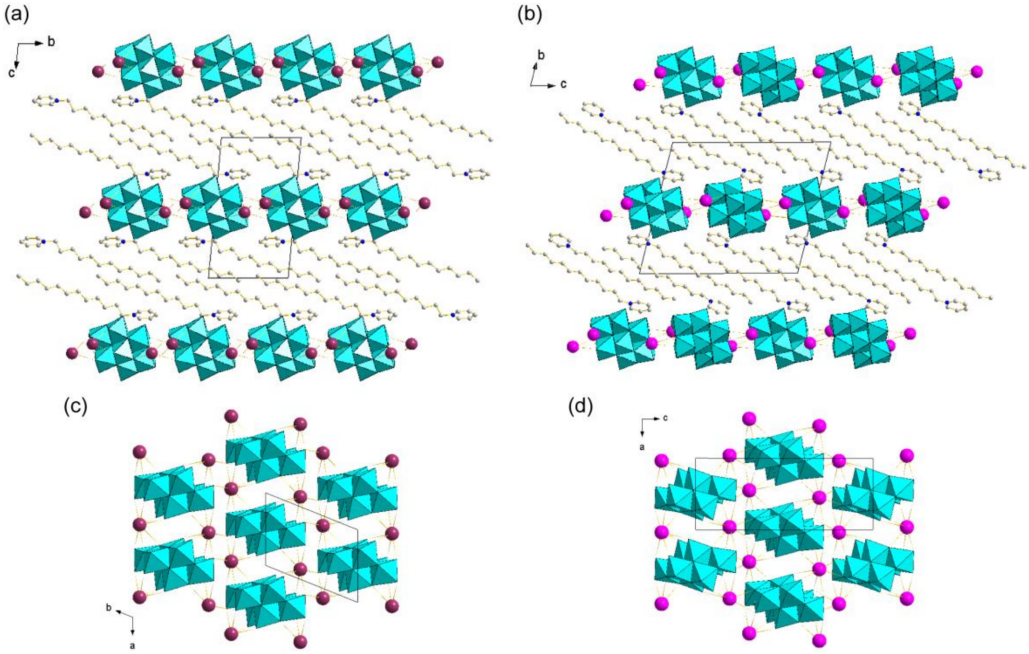

Figure 4. Crystal structures of C_{12}py-Rb-Mo_8 and C_{12}py-Cs-Mo_8 (C: gray, N: blue, Rb: plum, Cs: pink; β-Mo_8 in blue polyhedrons). H atoms and disordered atoms are omitted for clarity: (**a**) Packing diagram of C_{12}py-Rb-Mo_8 along the *a* axis; (**b**) Packing diagram of C_{12}py-Cs-Mo_8 along the *a* axis; (**c**) Molecular arrangements of C_{12}py-Rb-Mo_8 in the inorganic layers (*ab* plane); (**d**) Molecular arrangements of C_{12}py-Cs-Mo_8 in the inorganic layers (*ac* plane).

The C_{12}py-Rb-Mo_8 and C_{12}py-Cs-Mo_8 hybrid crystals were composed of alternately stacked β-Mo_8 monolayers and C_{12}py interdigitated bilayers. The layer periodicities were 17.5 Å for C_{12}py-Rb-Mo_8 and 16.8 Å for C_{12}py-Cs-Mo_8, respectively (Figure 4a,b). The inorganic layers consisted of the β-Mo_8 anions connected by Rb^+ or Cs^+, which held nine-fold coordination environment through terminal and bridging O atoms of three β-Mo_8 anions (Figure 4c,d). The bond distance was 2.85–3.21 Å (mean value: 3.03 Å) for Rb–O, and 3.06–3.41 Å (mean value: 3.21 Å) for Cs–O, respectively. The pyridine rings of C_{12}py were excluded from the inorganic layers formed by the densely connected β-Mo_8 anions and metal cations [41].

Although the C_{12}py-Rb-Mo_8 and C_{12}py-Cs-Mo_8 hybrid crystals held similar structures, there were some subtle differences. C_{12}py-Rb-Mo_8 had one crystallographically-independent β-Mo_8 anion, and C_{12}py-Cs-Mo_8 had two crystallographically-independent β-Mo_8 anions, leading to the different molecular conformation of β-Mo_8 in the inorganic layers (Figure 4c,d). As for the conformation of the C_{12}py surfactant, the dodecyl chains were partly interdigitated in the C_{12}py-Rb-Mo_8 hybrid crystals, while fully interdigitated in C_{12}py-Cs-Mo_8 (Figure 4a,b). This may lead to the longer interlayer distance of C_{12}py-Rb-Mo_8 (17.5 Å) than C_{12}py-Cs-Mo_8 (16.8 Å).

3.4. Yields of Metal Cation-Introduced Hybrid Crystals Relecant to Ion-Capturing Property

Metal cation-introduced hybrid crystals of C_{12}py-Rb-Mo_8 and C_{12}py-Cs-Mo_8 were obtained from the starting C_{12}py-Mo_8 hybrid crystals (Scheme 1b). The coexisting C_{12}py-Mo_8 hybrid crystal and metal cation in the crystallization solution will induce the formation of C_{12}py-Rb-Mo_8 and C_{12}py-Cs-Mo_8. This means that the C_{12}py-Mo_8 hybrid crystal can capture Rb^+ and Cs^+ from the solution into the solid phase as the C_{12}py-Rb-Mo_8 and C_{12}py-Cs-Mo_8 hybrid crystals. Therefore, the yield of C_{12}py-Rb-Mo_8 and C_{12}py-Cs-Mo_8 can be related to the ion-capturing property of C_{12}py-Mo_8 hybrid crystals.

The yield of C_{12}py-Rb-Mo_8 and C_{12}py-Cs-Mo_8 was investigated under various crystallization conditions. The keeping temperature was changed from 279 to 303 K (Figure 5). The obtained colorless solids or crystals were confirmed to be the C_{12}py-Rb-Mo_8 and C_{12}py-Cs-Mo_8 hybrid crystals by their IR spectra (Figure S4). The yield of C_{12}py-Rb-Mo_8 was almost constant at 25–30% in the considered temperature range. On the other hand, the yield of C_{12}py-Cs-Mo_8 was 35% at 279 K; however, this decreased drastically over 288 K to 12% at 303 K.

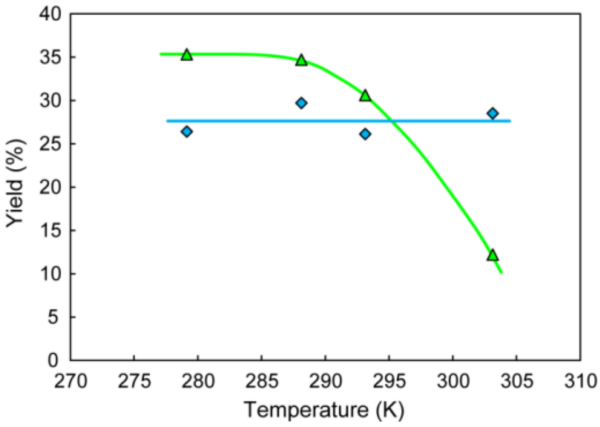

Figure 5. Yield of C_{12}py-Rb-Mo_8 and C_{12}py-Cs-Mo_8 hybrid crystals under various temperatures (blue diamonds: C_{12}py-Rb-Mo_8, green triangles: C_{12}py-Cs-Mo_8).

4. Discussion

The hybrid crystals of C_{12}py-Mo_8 and C_{12}py-Mo_8-AN were pseudopolymorphs (Figure 3). The emergence of the pseudopolymorphism was caused by the difference in the heating temperatures as shown in Scheme 1b. The lower heating temperature (308 K) and smaller difference (5 K) to the keeping temperature (303 K) provided milder crystallization conditions, resulting in the formation of C_{12}py-Mo_8 without crystallization solvent. On the other hand, the higher heating temperature (353 K) and larger difference (50 K) to the keeping temperature (303 K) caused severer crystallization conditions, resulting in the phase of C_{12}py-Mo_8-AN including crystallization solvent. These results suggest that C_{12}py-Mo_8 obtained under milder crystallization conditions was an energetically preferred phase, and that C_{12}py-Mo_8-AN formed under severer conditions was a kinetically preferred phase. This implication is consistent with the results that C_{12}py-Mo_8 was also formed by the gradual reoxidation of C_{12}py-red-Mo, which will slowly crystallize C_{12}py-Mo_8. From a structural aspect, the crystal structure and molecular conformation observed in C_{12}py-Mo_8-AN were similar to those in C_{16}py-α-Mo_8 hybrid crystals [39] except for the layer distance and the presence of crystallization solvent, while no similar phase to C_{12}py-Mo_8 was obtained for the C_{16}py-Mo_8 system.

The isomerization of α-Mo_8 anion to β-Mo_8 induced the introduction of metal into the hybrid crystals [41]. Rb^+ and Cs^+ were successfully incorporated when C_{12}py-Mo_8 was employed as the starting precipitate. The crystal structures and molecular conformations observed in C_{12}py-Rb-Mo_8 and C_{12}py-Cs-Mo_8 were similar to those in C_{16}py-Cs-Mo_8 [41]. The C_{16}py-Cs-Mo_8 hybrid crystal was obtained only as a mixture with low yield (<10%). However, C_{12}py-Rb-Mo_8 and C_{12}py-Cs-Mo_8 were able to isolate as a pure phase with

moderate yield (~30%). This will be because of higher solubility of C_{12}py-Mo_8 than C_{16}py-Mo_8 derived from the shorter hydrophobic alkyl chain.

As mentioned above, the C_{12}py-Mo_8 hybrid crystal can incorporate Rb^+ and Cs^+ cations from the solution phase into the solids to form the C_{12}py-Rb-Mo_8 and C_{12}py-Cs-Mo_8 hybrid crystals. This property renders it possible for utilizing C_{12}py-Mo_8 as absorbers capturing radioactive metal cations. Figure 5 shows the yields of C_{12}py-Rb-Mo_8 and C_{12}py-Cs-Mo_8 were approximately 30% based on the solid $RbNO_3$ or $CsNO_3$ in maximum, which suggests that approximately 30% of Rb^+ or Cs^+ could be removed from the solution phase. The removal of Rb^+ and Cs^+ will be an irreversible process: Rb^+ and Cs^+ in the solution phase were incorporated into the solid state, resulting in C_{12}py-Rb-Mo_8 and C_{12}py-Cs-Mo_8 crystals with rigid packing and low solubility. Therefore, the captured Rb^+ and Cs^+ could not be facilely released, and it seems difficult to reuse C_{12}py-Mo_8 as a metal-cation capturing material.

The moderate capturing rate (ca. 30%) of C_{12}py-Mo_8 will be due to the formation mechanism of C_{12}py-Rb-Mo_8 and C_{12}py-Cs-Mo_8 (Scheme 1a). The α-Mo_8 anions dissolved from the starting C_{12}py-Mo_8 solid isomerized to β-Mo_8 in acetonitrile, and sequentially reprecipitated with metal cations to form C_{12}py-Rb-Mo_8 and C_{12}py-Cs-Mo_8. The entire process is not a solid-state ion-exchange reaction, and less superior to well-established solid-state systems regarding the exchange rate and selectivity [11–13]. Changing the C_{12}py cation to an ionic-liquid surfactant may improve the capturing rate. Although the capturing property of C_{12}py-Mo_8 is not sufficient as toxic metal cation-capturing materials, the results presented here may open a new possibility of POM–surfactant hybrid materials.

Supplementary Materials: The following supporting information can be downloaded at: https://www.mdpi.com/article/10.3390/ma15072429/s1, Table S1: Crystallographic data for C_{12}py-Mo_8 prepared from C_{12}py-red-Mo; Figure S1: Measured and calculated powder X-ray diffraction patterns of C_{12}py-Mo_8 and related hybrid crystals. Measured patterns were obtained at ambient temperature. Calculated patterns were obtained from the structure revealed by single-crystal X-ray diffraction; Figure S2: Structural information of C_{12}py-Mo_8 hybrid crystal prepared by the reoxidation of C_{12}py-red-Mo; Figure S3: Crystal structure of C_{12}py-Mo_8 hybrid crystal prepared by the reoxidation of C_{12}py-red-Mo; Figure S4: IR spectra of metal cation-introduced C_{12}py-Mo_8 hybrid crystals obtained at various crystallization temperatures.

Author Contributions: Conceptualization, T.I.; methodology, J.K., K.S. and K.M.; formal analysis, T.I., J.K., K.M., S.O. and T.M.; investigation, J.K., K.S., K.M. and S.O.; resources, E.I. and H.N.; writing—original draft preparation, T.I.; writing—review and editing, T.I.; visualization, T.I., J.K., K.S. and K.M.; funding acquisition, T.I. All authors have read and agreed to the published version of the manuscript.

Funding: This research was funded by JSPS KAKENHI (grant numbers JP26410245 and JP21K05232), and the JSPS Core-to-Core Program ((grant number A31-4).

Institutional Review Board Statement: Not applicable.

Informed Consent Statement: Not applicable.

Data Availability Statement: Further details of the crystal structure investigation (CCDC 2153845-2153849) can be obtained free of charge via www.ccdc.cam.ac.uk/data_request/cif (accessed on 22 February 2022), or by emailing data_request@ccdc.cam.ac.uk, or by contacting The Cambridge Crystallographic Data Centre, 12 Union Road, Cambridge CB2 1EZ, UK; Fax: +44-1223-336033.

Acknowledgments: Synchrotron X-ray diffraction measurements were carried out at 2D Beamline, the Pohang Accelerator Laboratory (PAL) supported by Pohang University of Science and Technology (POSTECH). Tatsuhiro Kojima (Osaka University) and Masaki Kawano (Tokyo Institute of Technology) are gratefully acknowledged for their support on the measurements with synchrotron radiation at PAL, and Shinichi Koguchi (Tokai University) for helpful comments.

Conflicts of Interest: The authors declare no conflict of interest.

References

1. Kanatzidis, M.G. Discovery-Synthesis, Design, and prediction of chalcogenide phases. *Inorg. Chem.* **2017**, *56*, 3158–3173. [CrossRef] [PubMed]
2. Akinwande, D.; Huyghebaert, C.; Wang, C.-H.; Serna, M.I.; Goossens, S.; Li, L.-J.; Wong, H.-S.P.; Koppens, F.H.L. Graphene and two-dimensional materials for silicon technology. *Nature* **2019**, *573*, 507–518. [CrossRef] [PubMed]
3. Kato, T.; Uchida, J.; Ichikawa, T.; Sakamoto, T. Functional liquid crystals towards the next generation of materials. *Angew. Chem. Int. Ed.* **2018**, *57*, 4355–4371. [CrossRef]
4. Ogawa, M.; Kuroda, K. Photofunctions of intercalation compounds. *Chem. Rev.* **1995**, *95*, 399–438. [CrossRef]
5. Clemente-León, M.; Coronado, E.; Martí-Gastaldo, C.; Romero, F.M. Multifunctionality in hybrid magnetic materials based on bimetallic oxalate complexes. *Chem. Soc. Rev.* **2011**, *40*, 473–497. [CrossRef] [PubMed]
6. Smith, M.D.; Connor, B.A.; Karunadasa, H.I. Tuning the luminescence of layered halide perovskites. *Chem. Rev.* **2019**, *119*, 3104–3139. [CrossRef] [PubMed]
7. Whittingham, M.S. Lithium batteries and cathode materials. *Chem. Rev.* **2004**, *104*, 4271–4301. [CrossRef]
8. Goodenough, J.B.; Park, K.-S. The Li-ion rechargeable battery: A perspective. *J. Am. Chem. Soc.* **2013**, *135*, 1167–1176. [CrossRef]
9. Coronado, E.; Gómez-García, C.J. Polyoxometalate-based molecular materials. *Chem. Rev.* **1998**, *98*, 273–296. [CrossRef]
10. Vargas, B.; Rodríguez-López, G.; Solis-Ibarra, D. The emergence of halide layered double perovskites. *ACS Energy Lett.* **2020**, *5*, 3591–3608. [CrossRef]
11. Manos, M.J.; Kanatzidis, M.G. Metal sulfide ion exchangers: Superior sorbents for the capture of toxic and nuclear waste-related metal ions. *Chem. Sci.* **2016**, *7*, 4804–4824. [CrossRef] [PubMed]
12. Uchida, S. Frontiers and progress in cation-uptake and exchange chemistry of polyoxometalate-based compounds. *Chem. Sci.* **2019**, *10*, 7670–7679. [CrossRef] [PubMed]
13. Ishizaki, M.; Akiba, S.; Ohtani, A.; Hoshi, Y.; Ono, K.; Matsuba, M.; Togashi, T.; Kananizuka, K.; Sakamoto, M.; Takahashi, A.; et al. Proton-exchange mechanism of specific Cs+ adsorption via lattice defect sites of Prussian blue filled with coordination and crystallization water molecules. *Dalton Trans.* **2013**, *42*, 16049–16055. [CrossRef]
14. Long, D.-L.; Burkholder, E.; Cronin, L. Polyoxometalate clusters, nanostructures and materials: From self assembly to designer materials and devices. *Chem. Soc. Rev.* **2007**, *36*, 105–121. [CrossRef]
15. Proust, A.; Matt, B.; Villanneau, R.; Guillemot, G.; Gouzerh, P.; Izzet, G. Functionalization and post-functionalization: A step towards polyoxometalate-based materials. *Chem. Soc. Rev.* **2012**, *41*, 7605–7622. [CrossRef] [PubMed]
16. Misra, A.; Kozma, K.; Streb, C.; Nyman, M. Beyond charge balance: Counter-cations in polyoxometalate chemistry. *Angew. Chem. Int. Ed.* **2020**, *59*, 596–612. [CrossRef]
17. Sadakane, M.; Steckhan, E. Electrochemical properties of polyoxometalates as electrocatalysts. *Chem. Rev.* **1998**, *98*, 219–237. [CrossRef]
18. Martín-Caballero, J.; Wéry, A.S.J.; Reinoso, S.; Artetxe, B.; San Felices, L.; El Bakkali, B.; Trautwein, G.; Alcañiz-Monge, J.; Vilas, J.L.; Gutiérrez-Zorrilla, J.M. A robust open·framework formed by decavanadate clusters and copper(ii) complexes of macrocyclic polyamines: Permanent microporosity and catalytic oxidation of cycloalkanes. *Inorg. Chem.* **2016**, *55*, 4970–4979. [CrossRef]
19. Rosen, M.J.; Kunjappu, J.T. *Surfactants and Interfacial Phenomena*, 4th ed.; Wiley: Hoboken, NJ, USA, 2012; pp. 126–132.
20. Kronberg, B.; Holmberg, K.; Lindman, B. *Surface Chemistry of Surfactants and Polymers*, 1st ed.; Wiley: Chichester, UK, 2014; pp. 113–136.
21. Yin, P.; Li, D.; Liu, T. Solution behaviors and self-assembly of polyoxometalates as models of macroions and amphiphilic polyoxometalate-organic hybrids as novel surfactants. *Chem. Soc. Rev.* **2012**, *41*, 7368–7383. [CrossRef]
22. Wu, H.; Yang, H.-K.; Wang, W. Covalently-linked polyoxometalate–polymer hybrids: Optimizing synthesis, appealing structures and prospective applications. *New J. Chem.* **2016**, *40*, 886–897. [CrossRef]
23. Song, Y.-F.; Long, D.-L.; Ritchie, C.; Cronin, L. Nanoscale Polyoxometalate-Based Inorganic/Organic Hybrids. *Chem. Rec.* **2011**, *11*, 158–171. [CrossRef] [PubMed]
24. Li, B.; Li, W.; Li, H.; Wu, L. Ionic complexes of metal oxide clusters for versatile self-assemblies. *Acc. Chem. Res.* **2017**, *50*, 1391–1399. [CrossRef] [PubMed]
25. Nisar, A.; Wang, X. Surfactant-encapsulated polyoxometalate building blocks: Controlled assembly and their catalytic properties. *Dalton Trans.* **2012**, *41*, 9832–9845. [CrossRef] [PubMed]
26. Clemente-León, M.; Coronado, E.; Soriano-Portillo, A.; Mingotaud, C.; Dominguez-Vera, J.M. Langmuir–Blodgett films based on inorganic molecular complexes with magnetic or optical properties. *Adv. Colloid Interface Sci.* **2005**, *116*, 193–203. [CrossRef]
27. Zhang, G.; Ke, H.; He, T.; Xiao, D.; Chen, Z.; Yang, W.; Yao, J. Synthesis and characterization of new layered polyoxometallates-1,10-decanediamine intercalative nanocomposites. *J. Mater. Res.* **2004**, *19*, 496–500. [CrossRef]
28. Janauer, G.G.; Dobley, A.D.; Zavalij, P.Y.; Whittingham, M.S. Evidence for decavanadate clusters in the lamellar surfactant ion phase. *Chem. Mater.* **1997**, *9*, 647–649. [CrossRef]
29. Spahr, M.E.; Nesper, R. Anhydrous octamolybdate with trimethyl hexadecyl ammonium cations. *Z. Anorg. Allg. Chem.* **2001**, *627*, 2133–2138. [CrossRef]
30. Ito, T.; Sawada, K.; Yamase, T. Crystal structure of bis(dimethyldioctadecylammonium) hexamolybdate: A molecular model of Langmuir-Blodgett films. *Chem. Lett.* **2003**, *32*, 938–939. [CrossRef]
31. Ito, T. Inorganic–organic hybrid surfactant crystals: Structural aspects and functions. *Crystals* **2016**, *6*, 24. [CrossRef]

32. Nyman, M.; Ingersoll, D.; Singh, S.; Bonhomme, F.; Alam, T.M.; Brinker, C.J.; Rodriguez, M.A. Comparative study of inorganic cluster-surfactant arrays. *Chem. Mater.* **2005**, *17*, 2885–2895. [CrossRef]
33. Nyman, M.; Rodriguez, M.A.; Anderson, T.M.; Ingersoll, D. Two structures toward understanding evolution from surfactant-polyoxometalate lamellae to surfactant-encapsulated polyoxometalates. *Cryst. Growth Des.* **2009**, *9*, 3590–3597. [CrossRef]
34. Yin, P.; Wu, P.; Xiao, Z.; Li, D.; Bitterlich, E.; Zhang, J.; Cheng, P.; Vezenov, D.V.; Liu, T.; Wei, Y. A Double-tailed fluorescent surfactant with a hexavanadate cluster as the head group. *Angew. Chem. Int. Ed.* **2011**, *50*, 2521–2525. [CrossRef] [PubMed]
35. Zhu, L.; Chen, K.; Hao, J.; Wei, Z.; Zhang, H.; Yin, P.; Wei, Y. Synthesis and crystallization behavior of surfactants with hexamolybdate as the polar headgroup. *Inorg. Chem.* **2015**, *54*, 6075–6077. [CrossRef] [PubMed]
36. Rosnes, M.H.; Musumeci, C.; Yvon, C.; Macdonell, A.; Pradeep, C.P.; Sartorio, C.; Long, D.-L.; Pignataro, B.; Cronin, L. Exploring the interplay between ligand derivatisation and cation type in the assembly of hybrid polyoxometalate Mn-Andersons. *Small* **2013**, *9*, 2316–2324. [CrossRef] [PubMed]
37. Wang, Y.; Lin, X.; Huang, B.; Chen, W.; Xiao, Z.; Wu, P. The crystal packing, morphology and hydrophobicity of polyoxometalate-based amphiphilic materials. *Cryst. Eng. Comm.* **2020**, *22*, 2434–2438. [CrossRef]
38. Mubeena, S.; Annapareddy, G.; Meghana, N.; Sarma, M. Crystallographic and spectroscopic analysis of 9,10-bis-alkyl imidazolium anthracene hexatungstate supramolecular complexes. *J. Mol. Struct.* **2021**, *1243*, 130876. [CrossRef]
39. Ito, T.; Mikurube, K.; Abe, Y.; Koroki, T.; Saito, M.; Iijima, J.; Naruke, H.; Ozeki, T. Hybrid inorganic-organic crystals composed of octamolybdate isomers and pyridinium surfactant. *Chem. Lett.* **2010**, *39*, 1323–1325. [CrossRef]
40. Ito, T.; Mikurube, K.; Hasegawa, K.; Kurasawa, M.; Naruke, H.; Ozeki, T. Polyoxomolybdate-surfactant hybrid layered crystal with unusually long periodicity. *Chem. Lett.* **2011**, *40*, 626–628. [CrossRef]
41. Mikurube, K.; Hasegawa, K.; Matsumoto, T.; Kobayashi, J.; Naruke, H.; Ito, T. Isomerization-induced introduction of metal cations into polyoxomolybdate-surfactant hybrid crystals. *Inorg. Chem. Commun.* **2016**, *73*, 45–48. [CrossRef]
42. Klemperer, W.G.; Shum, W. Synthesis and interconversion of the isomeric α- and β-$Mo_8O_{26}{}^{4-}$ ions. *J. Am. Chem. Soc.* **1976**, *98*, 8291–8293. [CrossRef]
43. Himeno, S.; Niiya, H.; Ueda, T. Raman studies on the identification of isopolymolybdates in aqueous solution. *Bull. Chem. Soc. Jpn.* **1997**, *70*, 631–637. [CrossRef]
44. Cruywagen, J.J. Protonation, oligomerization, and condensation reactions of vanadate(V), molybdate(VI),and tungstate(VI). *Adv. Inorg. Chem.* **1999**, *49*, 127–182.
45. *CrystalClear*; Rigaku Corporation: Tokyo, Japan, 2014.
46. *CrysAlisPro*; Rigaku Oxford Diffraction: Tokyo, Japan, 2015.
47. *PROCESS-AUTO*; Rigaku Corporation: Tokyo, Japan, 2002.
48. Sheldrick, G.M. SHELXT—Integrated space-group and crystal structure determination. *Acta Crystallogr. Sect. A* **2015**, *71*, 3–8. [CrossRef] [PubMed]
49. Altomare, A.; Cascarano, G.; Giacovazzo, C.; Guagliardi, A. Completion and refinement of crystal structures with *SIR92*. *J. Appl. Crystallogr.* **1993**, *26*, 343–350. [CrossRef]
50. Sheldrick, G.M. A short history of SHELX. *Acta Crystallogr., Sect. A* **2008**, *64*, 112–122. [CrossRef]
51. *CrystalStructure 4.3*; Rigaku Corporation: Tokyo, Japan, 2017.
52. Román, P.; Gutiérrez-Zorrilla, J.M.; Esteban-Calderón, C.; Martínez-Ripoll, M.; García-Blanco, S. Synthesis, characterization and crystal structure of the anilinium β-octamolybdate dihydrate. *Polyhedron* **1985**, *4*, 1043–1046. [CrossRef]
53. Román, P.; San José, A.; Aranzabe, A.; Luque, A. Synthesis, solid state characterization and thermal behavior of some tert-butylammonium polymolybdates. *Thermochim. Acta* **1992**, *206*, 137–147. [CrossRef]
54. Chen, Y.; Shen, X.; Zhang, H.; Huang, C.; Cao, Y.; Sun, R. Synthesis, solid state characterization and thermal behavior of some tert-butylammonium polymolybdates. The structure and two-dimensional correlation infrared spectroscopy study of a new 2D polyoxomolybdate complex containing b-octamolybdate linked up by potassium ions: $(4,4'\text{-Hbpy})_2(K_2Mo_8O_{26})$. *Vib. Spectrosc.* **2006**, *40*, 142–147.
55. Courcot, B.; Adam, J.; Bridgeman, A.J. Structural and vibrational study of $[Mo_7O_{24}]^{6-}$ and $[W_7O_{24}]^{6-}$. *J. Phys. Chem. A* **2009**, *113*, 10540–10548. [CrossRef]